Permeability and effective slip in confined flows transverse to wall slippage patterns

Avinash Kumar, Subhra Datta, and Dinesh Kalyanasundaram

Citation: Physics of Fluids **28**, 082002 (2016);
View online: https://doi.org/10.1063/1.4959184
View Table of Contents: http://aip.scitation.org/toc/phf/28/8
Published by the American Institute of Physics

Articles you may be interested in

Effective slip and friction reduction in nanograted superhydrophobic microchannels
Physics of Fluids **18**, 087105 (2006); 10.1063/1.2337669

Geometric transition in friction for flow over a bubble mattress
Physics of Fluids **21**, 011701 (2009); 10.1063/1.3067833

On the scaling of the slip velocity in turbulent flows over superhydrophobic surfaces
Physics of Fluids **28**, 025110 (2016); 10.1063/1.4941769

Laminar and turbulent flows over hydrophobic surfaces with shear-dependent slip length
Physics of Fluids **28**, 035109 (2016); 10.1063/1.4943671

Microchannel flows with superhydrophobic surfaces: Effects of Reynolds number and pattern width to channel height ratio
Physics of Fluids **21**, 122004 (2009); 10.1063/1.3281130

Achieving large slip with superhydrophobic surfaces: Scaling laws for generic geometries
Physics of Fluids **19**, 123601 (2007); 10.1063/1.2815730



CrossMark click for updates

PHYSICS OF FLUIDS **28**, 082002 (2016)

Permeability and effective slip in confined flows transverse to wall slippage patterns

Avinash Kumar,[1] Subhra Datta,[1,a)] and Dinesh Kalyanasundaram[2]
[1]*Department of Mechanical Engineering, IIT Delhi, Hauz Khas, New Delhi 110016, India*
[2]*Center for Biomedical Engineering, IIT Delhi, Hauz Khas, New Delhi 110016, India*

(Received 2 February 2016; accepted 9 July 2016; published online 1 August 2016)

The pressure-driven Stokes flow through a plane channel with arbitrary wall separation having a continuous pattern of sinusoidally varying slippage of arbitrary wavelength and amplitude on one/both walls is modelled semi-analytically. The patterning direction is transverse to the flow. In the special situations of thin and thick channels, respectively, the predictions of the model are found to be consistent with lubrication theory and results from the literature pertaining to free shear flow. For the same pattern-averaged slip length, the hydraulic permeability relative to a channel with no-slip walls increases as the pattern wave-number, amplitude, and channel size are decreased. Unlike discontinuous wall patterns of stick-slip zones studied elsewhere in the literature, the effective slip length of a sinusoidally patterned wall in a confined flow continues to scale with both channel size and the pattern-averaged slip length even in the limit of thin channel size to pattern wavelength ratio. As a consequence, for sufficiently small channel sizes, the permeability of a channel with sinusoidal wall slip patterns will always exceed that of an otherwise similar channel with discontinuous patterns on corresponding walls. For a channel with one no-slip wall and one patterned wall, the permeability relative to that of an unpatterned reference channel of same pattern-averaged slip length exhibits non-monotonic behaviour with channel size, with a minimum appearing at intermediate channel sizes. Approximate closed-form estimates for finding the location and size of this minimum are provided in the limit of large and small pattern wavelengths. For example, if the pattern wavelength is much larger than the channel thickness, exact results from lubrication theory indicate that a worst case permeability penalty relative to the reference channel of ~23% arises when the average slip of the patterned wall is ~2.7 times the channel size. The results from the current study should be applicable to microfluidic flows through channels with hydrophobized/super-hydrophobic surfaces. *Published by AIP Publishing.* [http://dx.doi.org/10.1063/1.4959184]

I. INTRODUCTION

It is now appreciated that apart from gases[1] and polymer melts,[2] even small-molecule liquids governed by the Newtonian viscosity law slip past a solid surface.[3–9] In general, the fluid velocity has a flow-driving-force dependent non-zero value on a solid surface, in contradiction of the classical no-slip boundary condition of fluid mechanics.[6] Whether the microscopic contact of a flowing liquid is with a homogeneous and molecularly smooth solid[5] or with a set of solid molecules inter-spaced with molecules of another solid[10] or with gas molecules trapped in surface asperities of a solid,[9,11] a useful continuum-scale local measure of the extent of slippage is the distance behind the macroscopic solid surface at which the fluid velocity would vanish if it were linearly extrapolated; this measure is known as slip length[6] (Fig. 1).

The slip length, can be of the order of 10 nm–10 μm.[8,12,13] Since a large slip length corresponds to reduced frictional resistance to flow, employing large-slip-length surfaces to microfluidic flows,

a)Electronic mail: subhra-datta@iitd.ac.in

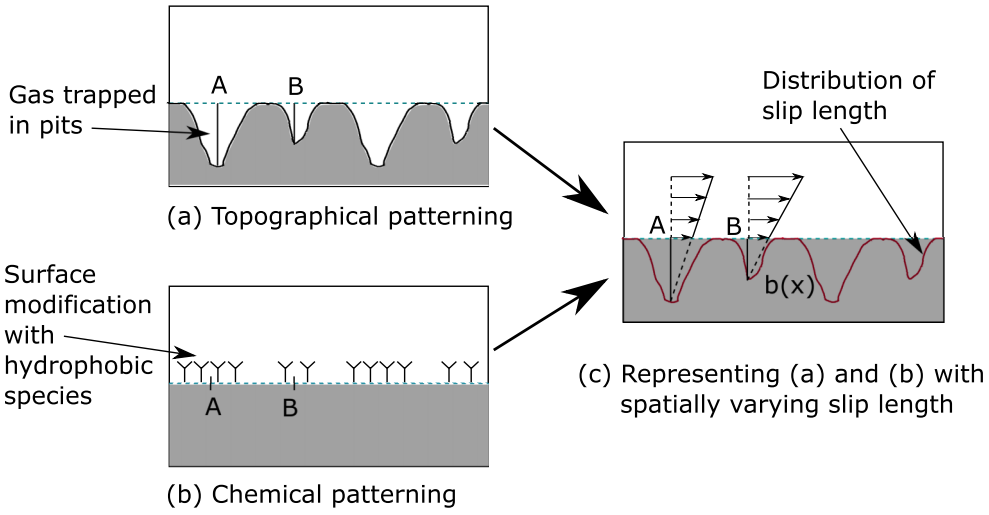


FIG. 1. Schematic representation of spatially varying slip (right) arising from topographical (top left) and chemical patterning (top right).

where the micro-/nano-channels have comparable dimensions,[14–17] will have energy saving consequences.[17,18] However, a surface with a uniformly large slip length[17,19] is difficult to realize.[11,20] Instead, surfaces with large slip for water can be engineered by introducing a hydrophobic phase into the surface, either via air trapped in the Cassie state[11] within nanostructures such as pillars/ridges of suitable dimensions[15,21] (as shown on the top left pane of Fig. 1), or via chemical rather than topographical modification of the surface[10,22] (as shown on the bottom left pane of Fig. 1). For the purposes of fluid dynamic modelling of their frictional behaviour, either kinds of surfaces can be conveniently replaced by a flat surface with a non-uniform distribution of slip lengths, as shown schematically on the right pane of Fig. 1. For a topographically patterned surface with gas "bubbles" trapped in surface pits, this approach, which predicts a proportionality between local slip and local depth of the pits (Fig. 1), can be justified on scaling grounds, given that a large viscosity contrast exists between the trapped gas phase and liquid.[23,24] Note, however, that this approach leaves unresolved the local details of liquid-gas menisci.[25]

Aside from reduced drag in comparison to surfaces with no slippage, flow over surfaces with slippage patterns can have a tensorial/anisotropic response to applied forces,[20] a phenomenon of interest to both microfluidic mixing[23,26] and microfluidic separations.[27] Both flows *over* such surfaces[28–30] and flows *confined by* such surfaces[31–34] (as in nanochannels) may be of interest. The current work concerns the latter, in view of its technological relevance to microfluidics.

The distribution of slip length on a surface, although needed to predict its frictional properties, is usually not accessible to measurements.[6,35] Instead, measurements can access fluid dynamic variables on a much courser scale, such as the drag per unit pitch for a periodically repeating surface pattern[6,35] or the pressure drop over a periodically repeating microchannel span.[32,36,37] To relate these course-grained variables to the local variables of continuum-scale fluid mechanics, homogenized measures such as effective slip length for a surface[20,38–40] and the (effective) hydraulic permeability for a channel[32,36,37] have been developed in the literature. The prediction of these effective measures of slip from a postulated distribution of local slip length on a surface is therefore an important modelling task.[28,38,41,42]

The theoretical work on the effect of spatial variations in slip length and/or prediction of corresponding effective slip can be divided into studies that do or do not address flow confinement. In the former category, free shear flow over a single patterned surface has been considered by several authors,[30,40,41,43–46] whereas Bahga *et al.*[29] consider electro-osmotic flow. Free shear flow corresponds to an important limiting situation for the confined pressure-driven flow to be studied in this work, wherein agreement with the results from Asmolov *et al.*,[30] Six and Kamrin[45] will be checked.

Confined flows have been studied by several authors.[31–34,37,42,47,48] Of these studies, Feuillebois *et al.*,[32] Ng and Zhou,[34] and Feuillebois *et al.*[37] study the limiting situation of the ratio of channel thickness being much smaller than the patterning wavelength in the sense of Hele-Shaw or lubrication theory.[49] The theoretical model to be developed in the current study will apply to arbitrary specification of this ratio, although (a) reduction to lubrication theory for small values of this ratio will be verified, and (b) certain new closed form results will be derived from lubrication theory to understand scaling behaviours, the effect of channel size, and misalignment between wall slip patterns.

Theoretical models also differ in terms of whether they are formulated for a (possibly) continuous distribution[30,31,33,42,44–46,50] of slip length or start with an assumed discontinuous slip-stick pattern of slippage.[28,32,34,37,38,41,43,47] Although the latter kind of patterned slip may appear to be a good first approximation to experimental situations where air bubbles are trapped in topographical nano-patterns,[15,51] continuous variation in slip may have the advantage of having lower dissipation and therefore better friction reduction.[30] Further, chemical gradients[10] in hydrophobicity produce continuous patterns. However, it should be noted that the surfaces with continuous variation of slip length may be extremely difficult to realize with currently established fabrication and characterization technologies.[6,8,52] In the current study, a continuous sinusoidal variation of slip will be used and certain scaling laws emphasizing its advantage over discontinuous patterns will be brought out.

Among the studies that employ a continuous variation of slip length, specifically a sinusoidal distribution of slip is used by several authors.[30,31,33,42,45,53,54] However, the analyses of Hendy *et al.*,[31] Ghosh and Chakraborty,[33] Choudhary *et al.*,[42] and Zhao and Yang[54] are limited to confined flows with small amplitude patterning. The unconfined shear flow is studied by Asmolov *et al.*[30] and Six and Kamrin.[45] Although the model of Six and Kamrin[45] corresponds to a specific pattern amplitude of the pattern studied in Asmolov *et al.*,[30] the former provides an important closed form estimate of effective slip unavailable from elsewhere.

In addition to analytical approaches, problems with spatial variations in the degree of slippage have been modelled numerically on molecular/meso-scale using particle dynamics based simulations,[46,55] as well as on the continuum-scale. Continuum scale numerical simulations proceed through approaches such as finite-difference/volume,[56] finite-element,[42] point collocation,[57] and Lattice-Boltzmann[47,58] methods; because of their discretization requirements, these methods have only algebraic decay of errors as the number of nodes in the grid is increased. The semi-analytical continuum-scale solution procedure adopted in this work to analyze slippage patterning has faster decay of errors with its truncation parameter than the above-discussed continuum-scale methods and involves a much smaller computational cost than all the above-discussed simulations.

Pressure-driven flow in a planar microchannel with a sinusoidal distribution of slippage on one/both of its works is studied theoretically in this work. The theory is valid for arbitrary values of channel thickness, pattern wavelength, pattern amplitude, and the average slip length of the pattern. Important limiting situations corresponding to certain limiting values for the ratios of these parameters are studied, along with comparison from the literature. Two model problems are solved sequentially for the local velocity field using a spectrally accurate semi-analytical approach based on Fourier series representation of the periodic flow field. In the first problem, the plane channel has one no-slip wall, a situation of experimental interest since this wall configuration avoids issues of alignment.[37] In the second problem, the microchannel has aligned opposite walls of patterned slippage. Global measures such as effective slip length of the individual walls and the (effective) hydraulic permeability of the micro-/nanochannel[32,36,37] are then calculated for either problems. The effective slip of the sinusoidal pattern scales differently than discontinuous stick-slip patterns with variables such as channel height and average slip. A new global measure termed patterned channel to unpatterned channel permeability ratio is also defined and evaluated; the dependence of this measure on the pattern characteristics reveals a certain design issue that may arise regarding choosing the cross-dimension of the planar micro-/nano-channel. This issue is addressed through closed form analysis. Further, using scaling arguments and this new measure, significant distinctions are brought out between the fluid dynamic behaviour of (a) plane channels with one/two patterned walls and (b) continuous and discontinuous patterns, especially with respect to miniaturization.

The article is organized into a section on theoretical modelling of the flow field and effective slip, followed by one (Sec. III) discussing the corresponding results. To study an important limiting situation, reference is made in either sections to the Appendix. Finally, conclusions are presented and the scope for future work is discussed.

II. THEORETICAL FORMULATION

The flow through a channel with transverse stripes on one (Fig. 2(a)) or more (Fig. 2(b)) of its walls will be considered here. The width and length of the channel are much larger than the thickness h. The wall(s) are patterned with transverse stripes, which means the patterning direction is perpendicular to the direction of flow. In contrast to longitudinal stripes,[30] transverse stripes produce a bidirectional flow field. Note that longitudinal stripes are known to be more permeable than transverse stripes,[20,37] thereby resulting in an anisotropic flow response to applied forces of channels with inclined stripes.[32] The permeability and flow-field of channels with longitudinal stripes for arbitrary values of pattern wavelength, amplitude, and channel size have been studied elsewhere.[59]

The slip length (b) is patterned according to

$$b(x) = b_0\left(1 + \alpha\cos\left(\frac{2\pi x}{L}\right)\right) \tag{1}$$

in the coordinate system of Figs. 2(a) and 2(b). Here, α is the dimensionless amplitude of the pattern, L is its wavelength, and b_0 the pattern-averaged slip length or "base slip length." In Fig. 2(a), one of the walls (here, the top wall) is patterned with the above slip distribution and the other wall is non-slipping. In Fig. 2(b), both the top and bottom walls are patterned with the above slip distribution. For the sake of conciseness, the problem shown in Fig. 2(a) will be termed Problem I, and that shown in Fig. 2(b) will be termed Problem II. The practical relevance of Problem I is that it avoids difficulties from misalignment of the surfaces that might occur in an experimental realization of Problem II.[37] It is possible that in an actual experimental situation, the patterned surface may be placed below the un-patterned surface, unlike in Fig. 2. Since gravity effects can be neglected in microscale liquid flows,[14] the flow field should not be affected by this detail. The co-ordinate system and the wall location in Fig. 2 are chosen for later analytical convenience.

Referring to Fig. 2 and Eq. (1), the flow field and the overall pressure drop in the channel are completely determined in Problems I and II by prescription of the flow-rate Q, the channel height h, the fluid viscosity μ, the pattern base slip b_0, the dimensionless pattern amplitude α, and the pattern wavelength L. Certain global characteristics of the resultant flow will be defined below.

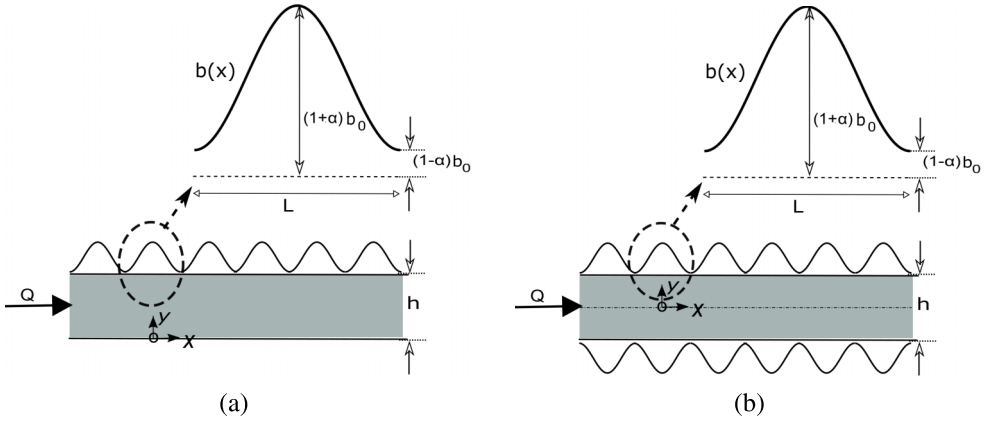


FIG. 2. Flow of flow-rate Q through a plane channel of thickness h with patterned slip on one/more of its walls. For the channel in pane (a), the top wall is patterned with the slip distribution given by Eq. (1) and the bottom wall is non-slipping. For the channel in pane (b), both the top and bottom walls are patterned with the slip distribution given by Eq. (1) (shown as insets). The pattern wavelength is L, the pattern-averaged slip length is b_0, and the pattern amplitude is αb_0. (a) Problem I: plane channel with one slip-patterned and one no slip wall. (b) Problem II: plane channel with both walls slip-patterned.

For a Newtonian fluid slipping with local velocity u_s and local shear strain $\frac{\partial u}{\partial n}|_s$ over a stationary planar solid surface (s) with a periodic slip distribution of wavelength L, b_{eff} can be defined[40] in terms of spatial averages $\langle \ldots \rangle = 1/L \int_{-L/2}^{L/2} \ldots dx$ over one wavelength along the patterning direction (x) as follows:

$$b_{eff} = \frac{\langle u_s \rangle}{\left\langle \frac{\partial u}{\partial n}|_s \right\rangle}. \tag{2}$$

Here, n is a co-ordinate normal to the wall directed from fluid to solid side. Given that $b_0 = \langle b \rangle$ in Eq. (1), the ratio b_{eff}/b_0 shows the departure of effective slip from average slip. Further, an unpatterned surface ($\alpha = 0$) has a slip length b_0, as per the same equation. For $\alpha \neq 0$, b_{eff}/b_0 should be less than unity, since patterning introduces viscous dissipation into the flow.[20] This ratio will be used to characterize the effect of patterning on an *individual channel wall*.

The (effective) hydraulic permeability[20] (κ) is a property of the *channel* defined to be flow rate per unit cross-sectional area per unit pressure drop along the channel. This measure can be considered to be an adaptation from the corresponding quantity defined in the hydrodynamic theory of porous media.[60] The dimensionless permeability K_{eff}[20] of a channel with slip (patterned on both walls) is defined to be the ratio $K_{eff} = \frac{\kappa}{\kappa_{NS}}$ of κ to the hydraulic permeability $\kappa_{NS} = h^2/(12\mu)$ of a reference channel with no slip (NS) on all walls. Given that for an unpatterned ($\alpha = 0$) channel, the effective slip length is the same as average slip length $b_0 = \langle b \rangle$, a dimensionless reference permeability K_0 can be defined to be the dimensionless permeability of an unpatterned channel with uniform pattern-averaged slip on *corresponding* walls. Then, with respect to Problems I and II, permeability can be connected to effective slip[20,37,47] as follows:

$$\begin{aligned} K_{eff/0} &= \left(\frac{1 + 4\frac{b_{eff/0}}{h}}{1 + \frac{b_{eff/0}}{h}} \right) \quad \text{for Problem I} \\ &= \left(1 + 6\frac{b_{eff/0}}{h} \right) \quad \text{for Problem II.} \end{aligned} \tag{3}$$

In the above equation, the suffix *eff* or 0 should be used accordingly as a patterned and un-patterned channel of effective slip given by b_{eff} or uniform slip given by b_0 is under consideration. The supplementary material[61] provides a detailed derivation of this equation for any periodic slip pattern by employing a formal axial averaging procedure of the local equations of fluid flow over one wavelength of pattern. The values of $K_{eff/0}$ can range between 1 and 4 for Problem I, and 0 and ∞ for Problem II. These two limits correspond to $b_{eff/0}/h = 0$ and $b_{eff/0}/h \to \infty$. Further, K_{eff} cannot exceed K_0.[20]

In this study, it will be convenient to study the effect of patterning through a variable that is normalized to unity for channels with un-patterned walls, regardless of the specific slip/no-slip wall configuration such as in Figs. 2(a) and 2(b). Accordingly, a new measure (R) termed patterned channel to un-patterned channel permeability ratio or in short permeability ratio will be defined. The permeability ratio is defined as the factor by which the permeability of the patterned channel departs from that of an un-patterned reference channel of the same period averaged slip length $\langle b \rangle$. Since, in this study, $\langle b \rangle = b_0$ corresponding to an un-patterned channel, it follows that

$$R = \frac{K_{eff}}{K_0}. \tag{4}$$

Unlike K_{eff}, R cannot exceed unity.

For Problems I and II, Eq. (3) can be used in the above equation, then R takes the form,

$$\begin{aligned} R &= \left(\frac{1 + 4\frac{b_{eff}}{h}}{1 + \frac{b_{eff}}{h}} \right) \left(\frac{1 + \frac{b_0}{h}}{1 + 4\frac{b_0}{h}} \right) \quad \text{for Problem I} \\ &= \frac{1 + 6\frac{b_{eff}}{h}}{1 + 6\frac{b_0}{h}} \quad \text{for Problem II.} \end{aligned} \tag{5}$$

The lowest R will occur when $b_{eff}/h = 0$ but $b_0/h \to \infty$. Therefore, R can vary between 1/4 and 1 in Problem I, and 0 and 1 in Problem II.

The remainder of this section will solve for the local flow patterns and evaluate the effective slip in both Problems I and II, in that order. Evaluation of the flow field and the measures b_{eff}, K_{eff}, and R for specific situations will be taken up in Sec. III. Inertial and gravity effects on fluid flow will be neglected, which is suitable for most microfluidic applications.[14]

A. Problem I: Transverse flow in channel with one non-slipping wall and one wall with sinusoidally striped slip

1. Calculation of the flow field

Referring to Fig. 2(a), the flow field is governed by the equations of steady incompressible Stokes flow, the appropriate slip/no-slip and impervious wall boundary conditions, and the requirement of meeting a prescribed flow-rate Q. Using the scales L for the axial (x) and cross-channel (y) co-ordinates, Q/L for the velocities u in the x direction and v in the y direction, and $\mu Q/L^2$ for pressure p, the non-dimensionalized form of these equations can be written in corresponding dimensionless variables X, Y, U, V, and P as follows:

$$\frac{\partial^2 U}{\partial X^2} + \frac{\partial^2 U}{\partial Y^2} = \frac{\partial P}{\partial X}, \tag{6}$$

$$\frac{\partial^2 V}{\partial X^2} + \frac{\partial^2 V}{\partial Y^2} = \frac{\partial P}{\partial Y}, \tag{7}$$

$$\frac{\partial U}{\partial X} + \frac{\partial V}{\partial Y} = 0. \tag{8}$$

The boundary conditions are

$$U\Big|_{Y=0} = 0, \tag{9}$$

$$U\Big|_{Y=1/\lambda} + \beta(X)\frac{\partial U}{\partial Y}\Big|_{Y=1/\lambda} = 0, \tag{10}$$

and

$$V\Big|_{Y=0} = V\Big|_{Y=1/\lambda} = 0. \tag{11}$$

Here, $\lambda = L/h$ is a dimensionless parameter, and the dimensionless slip distribution $\beta(X)$ is given by

$$\beta(X) = \beta_0 \left(1 + \alpha \cos\left(2\pi X\right)\right), \tag{12}$$

where $\beta_0 = b_0/L$.

Further, since $Q = \int_0^h u dy$, in dimensionless form,

$$\int_0^{1/\lambda} U dY = 1. \tag{13}$$

Introducing the stream-function ψ defined to satisfy Eq. (8) through the relations $U = \frac{\partial \psi}{\partial Y}$ and $V = -\frac{\partial \psi}{\partial X}$, Eqs. (6) and (7) can be combined into a single equation

$$\frac{\partial^4 \psi}{\partial X^4} + 2\frac{\partial^2}{\partial X^2}\left(\frac{\partial^2 \psi}{\partial Y^2}\right) + \frac{\partial^4 \psi}{\partial Y^4} = 0. \tag{14}$$

Due to its definition, ψ can be known only up to a constant; therefore, $\psi(X, 0) = 0$ on the bottom impervious wall is chosen for convenience. With this choice Eq. (13) becomes

$$\psi(X, 1/\lambda) = 1. \tag{15}$$

The no-slip condition on the unpatterned bottom wall of Fig. 2(a) becomes

$$\frac{\partial \psi}{\partial Y}\Big|_{Y=0} = 0. \tag{16}$$

The slip condition on the patterned top wall becomes

$$\frac{\partial \psi}{\partial Y}\Big|_{Y=1/\lambda} + \beta(X)\frac{\partial^2 \psi}{\partial Y^2}\Big|_{Y=1/\lambda} = 0. \tag{17}$$

Following an approach similar to that for free shear flow,[30] a stream function (ψ) satisfying Eq. (14), (15), and $\psi(X,0) = 0$ has the following Fourier expansion in X:

$$\psi = a_1 Y^3 + (\lambda^2 - \frac{a_1}{\lambda})Y^2 + \sum_{n=1}^{\infty} C_n F_n(Y)\cos(k_n X), \tag{18}$$

where

$$F_n(Y) = (1 - \lambda Y + Y k_n \coth(\frac{k_n}{\lambda}))\sinh(k_n Y) - k_n Y \cosh(k_n Y). \tag{19}$$

To find the set of constants C_n ($n \geq 1$) and a_1, the slip boundary condition on the patterned bottom wall given by Eq. (17) must be used. Substituting Eq. (18) into this equation, after the use of a trigonometric identity, the following is obtained:

$$\begin{aligned}
&\left[\frac{4a_1\beta_0}{\lambda} + 2\lambda^2\beta_0 + (\frac{a_1}{\lambda^2} + 2\lambda) + \frac{\alpha\beta_0 C_1 F_1''(1/\lambda)}{2}\right] \\
&+ \left[\beta_0 C_1 F_1''(1/\lambda) + \frac{4a_1\beta_0\alpha}{\lambda} + 2\alpha\beta_0\lambda^2 + \frac{\alpha\beta_0}{2}C_2 F_2''(1/\lambda) + C_1 F_1'(1/\lambda)\right]\cos(k_1 X) \\
&+ \sum_{n=2}^{\infty}\left[\beta_0 C_n F_n''(1/\lambda) + \frac{\alpha\beta_0}{2}C_{n-1}F_{n-1}''(1/\lambda) + \frac{\alpha\beta_0}{2}C_{n+1}F_{n+1}''(1/\lambda) + C_n F_n'(1/\lambda)\right]\cos(k_n X) = 0.
\end{aligned} \tag{20}$$

On the left hand side of above equation, the coefficients of all the bases functions ($\cos(k_n), k_n = 2\pi n, n \geq 0$) can be equated to zero, resulting in the following problem obtained for the yet unknown coefficients.

For $n > 1$,

$$e_{n-1}C_{n-1} + d_n C_n + e_{n+1}C_{n+1} = 0, \tag{21}$$

where (following a notation similar to Asmolov *et al.*[30])

$$e_n = \frac{\beta_0\alpha F_n''(1/\lambda)}{2} \quad \text{and} \quad d_n = \beta_0 F_n''(1/\lambda) + F_n'(1/\lambda) \tag{22}$$

for $n = 1$,

$$[d_1 - \frac{4\lambda\beta_0\alpha e_1}{(1 + 4\lambda\beta_0)}]C_1 + e_2 C_2 = \frac{6\lambda^2\beta_0\alpha}{(1 + 4\lambda\beta_0)}, \tag{23}$$

for $n = 0$,

$$a_1 = -\frac{\lambda^2(4\lambda + 4\lambda^2\beta_0 + \beta_0\alpha C_1 F_1''(1/\lambda))}{2(1 + 4\lambda\beta_0)}. \tag{24}$$

Eq. (18) and correspondingly the equation system given by Eq. (21) can be truncated after N terms/equations; since $\beta(x)$ and all its derivatives are continuous, the corresponding truncation error will decay at an exponentially fast rate with N.[62] Eqs. (21) and (23) will form an $N \times N$ linear system that can be solved for C_ns by inversion of the corresponding tri-diagonal matrix using Thomas algorithm.[63] Using C_1 in Equation (24), a_1 can be obtained. The a_1, C_n s thus obtained and $F_n(Y)$ obtained using Eq. (19) can be substituted in Eq. (18) to obtain $\psi(X,Y)$ which describes the dimensionless flow-field in the channel shown in Fig. 2. Depending on the wave number of the pattern studied, truncating the system of equations to $O(10) - O(10^2)$ equations was found to be sufficient to allow the calculated slip length to converge up to at least seven digits. The convergence of the coefficients C_1 and C_2 with number of equations is included in the supplementary material.[61] Utilizing Shanks transformation,[64] the series was summed after truncation to $O(10)$ terms. Because of the exponentially fast decay of errors, the current method for obtaining the flow-field is more accurate than methods that require discretization on a grid such as finite-difference/volume,[56] finite-element,[42] point collocation,[57] and Lattice-Boltzmann[47,58] methods and therefore have only algebraic decay of errors as the number of nodes in the grid is increased.

2. *Effective slip length*

The dimensionless form of Eq. (2) applicable to the current problem is

$$\beta_{eff} = -\frac{\left\langle U \right\rangle\Big|_{Y=1/\lambda}}{\left\langle \frac{\partial U}{\partial Y} \right\rangle\Big|_{Y=1/\lambda}}. \tag{25}$$

Using $U = \dfrac{\partial \Psi}{\partial Y}$, $\dfrac{\partial U}{\partial Y} = \dfrac{\partial^2 \Psi}{\partial Y^2}$ and with ψ given by Eq. (18), the definition of the dimensionless wavelength-average $\langle \ldots \rangle$ as $\int_{-1/2}^{1/2} \ldots dX$,

$$\left\langle U \right\rangle = 3a_1 Y^2 + 2(\lambda^2 - \frac{a_1}{\lambda})Y, \tag{26}$$

$$\left\langle \frac{\partial U}{\partial Y} \right\rangle = 6a_1 Y + 2(\lambda^2 - \frac{a_1}{\lambda}). \tag{27}$$

Using Eqs. (26) and (27) in Eq. (25), the effective slip length becomes

$$\beta_{eff} = -\frac{(a_1 + 2\lambda^3)}{\lambda(4a_1 + 2\lambda^3)}, \tag{28}$$

where a_1 can be calculated from Eq. (24), once the equation system given by Eqs. (21)-(23) is solved.

B. Problem II: Transverse flow in a channel with sinusoidally striped slip on both walls

Referring to Fig. 2(b), the flow field must be symmetric around the axis of symmetry $y = 0$, so it is sufficient to solve the problem in the upper half-channel. The dimensionless governing equations for the stream-function ψ are the same as in Sec. II A. However, the boundary conditions differ in three respects as follows:

1. Since U must be an even function of Y from symmetry considerations, the boundary condition at $Y = 0$ is

$$\frac{\partial^2 \psi}{\partial Y^2}\Big|_{Y=0} = 0 \tag{29}$$

rather than $\frac{\partial \psi}{\partial Y}\Big|_{Y=0} = 0$ as in Eq. (16).

2. Because the wall is located at $Y = \frac{1}{2\lambda}$ in Problem II, Eq. (17) is replaced by

$$\frac{\partial \psi}{\partial Y}\Big|_{Y=1/2\lambda} + \beta(X)\frac{\partial^2 \psi}{\partial Y^2}\Big|_{Y=1/2\lambda} = 0. \tag{30}$$

3. Because the half-channel accommodates half the flowrate, and $Y = 0$ can be taken as the streamline $\psi = 0$

$$\psi(X, 1/2\lambda) = \frac{1}{2}. \tag{31}$$

Following a solution procedure, very similar to that for Problem I, the flow-field for Fig. 2 is found to have the stream-function

$$\psi = a_1 Y^3 + (\lambda - \frac{a_1}{4\lambda^2})Y + \sum_{n=1}^{\infty} C_n F_n(Y) \cos(k_n X), \tag{32}$$

where

$$F_n(Y) = Y \cosh(k_n Y) - \frac{1}{2\lambda} \coth(\frac{k_n}{2\lambda}) \sinh(k_n Y). \tag{33}$$

The constants C_ns and a_1 in the above equation can be obtained via inversion of a truncated coefficient matrix as before. For Problem II: for $n > 1$,

$$e_{n-1}C_{n-1} + d_n C_n + e_{n+1}C_{n+1} = 0, \tag{34}$$

where

$$e_n = \frac{\beta_0 \alpha F_n''(1/2\lambda)}{2} \quad \text{and} \quad d_n = \beta_0 F_n''(1/2\lambda) + F_n'(1/2\lambda). \tag{35}$$

For $n = 1$,

$$[d_1 - \frac{3\lambda\beta_0\alpha e_1}{(1+6\lambda\beta_0)}]C_1 + e_2 C_2 = \frac{6\lambda^2\beta_0\alpha}{(1+6\lambda\beta_0)}, \tag{36}$$

for $n = 0$,

$$a_1 = \frac{-\lambda^2(2\lambda + \beta_0\alpha C_1 F_1''(1/2\lambda))}{(1+6\lambda\beta_0)}. \tag{37}$$

The effective slip length is given by

$$\beta_{eff} = -\frac{(a_1 + 2\lambda^3)}{6a_1\lambda}. \tag{38}$$

The symmetry boundary condition in Eq. (29) can also be interpreted as the interface condition on a liquid sharing a flat interface with a phase of much lower viscosity than the liquid such as a gas/vapour. Therefore, the flow-field and the effective slip length in a liquid layer of height $h/2$, on one side of which is a solid surface with patterned slip and on the other side of which is an axially continuous flat layer of gas, have exactly the same mathematical form as Problem II studied in this section, under the assumption that deformation of the initially planar free surface does not arise due to interfacial instabilities.[65] Such a gas layer being a perfectly slipping surface, if stabilized will be of advantage for friction reduction.[16]

III. RESULTS AND DISCUSSION

Since the current model is applicable for channels of arbitrary thickness to pattern wavelength ratios, reference will be made in this section to the two limiting situations of thin and thick channels (in relation to wall pattern wavelength), corresponding dimensionlessly to $\lambda \gg 1$ and $\lambda \ll 1$. The theory for $\lambda \gg 1$ corresponds to lubrication theory and the relevant key results are derived in the Appendix. The estimate (R_{LT}) of the permeability ratio R from lubrication theory is given by Eq. (A8) for Problem I (Fig. 2(a)) and Eq. (A10) for Problem II. The limit $\lambda \ll 1$, when b_0/L is prescribed, corresponds to the semi-analytical theory developed in the literature[30] for an isolated surface with sinusoidal stripes.

The typical presentation of a figure in this section will involve results for Problem I (Fig. 2(a)) on its left pane and those from Problem II (Fig. 2(b)) on its right pane. Unlike in the equations of Secs. I and II, in figures of the current section, it will be convenient to represent the dependent and independent dimensionless variables in terms of dimensional parameters. For example, the various dimensionless slip length variables $\beta_0, \lambda\beta_0, \beta_{eff}/\beta_0$ and the dimensionless velocity variable U/λ will be represented as $b_0/L, b_0/h, b_{eff}/b_0$, and uh/Q, respectively.

Fig. 3 shows the variation of the permeability ratio (R) with the dimensionless amplitude. Since the channel size to slip ratio $b_0/h = 1$ is prescribed in this situation, on each pane of the figures, the variation of R can more simply be interpreted as variation of the corresponding dimensionless channel permeability ($R \propto K_{eff}$ in Eq. (4)), and the variation of λ as that of the pattern wavelength. Increasing the pattern amplitude degrades the channel permeability. Shorter the wavelength of the channel, stronger is the magnitude as well as amplitude-sensitivity of this effect. In the long wave limit, the estimated R is in good agreement with the corresponding estimates from lubrication theory obtained using Eqs. (A8) and (A10). Comparing across the two panes, the permeability of the channel in Problem II relative to the corresponding unpatterned channel is affected more strongly by patterning; this is because the no-slip wall in Problem I is essentially an unpatterned surface.

Fig. 4 considers the variation of b_{eff}/b_0 with pattern amplitude. This dimensionless parameter is a measure of the effect of patterning on a single channel wall rather than the entire channel.

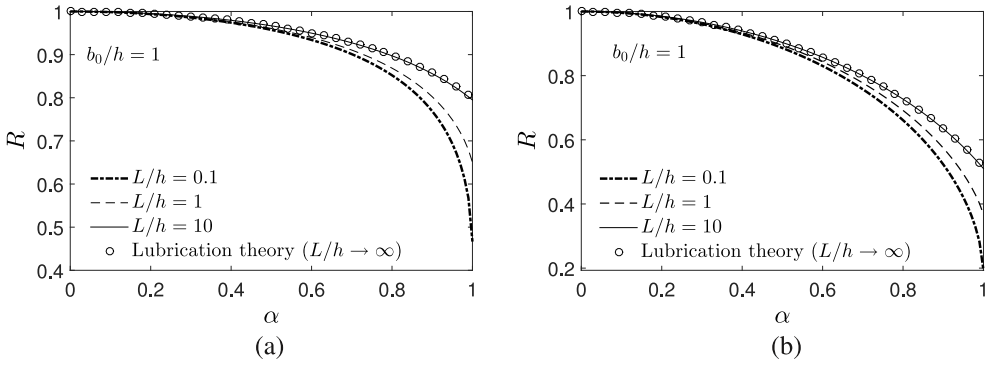


FIG. 3. Variation of the ratio of permeability of the patterned channel to that of unpatterned channel with amplitude (α) of patterning for various L/h ratios, corresponding to different wavelengths. The symbols correspond to the closed-form prediction from lubrication theory given by Eqs. (A8) and (A10). Problem II is for plane channel with both walls slip-patterned (Fig. 2(b)). (a) Problem I. (b) Problem II.

On studying the curves shown in this figure, it is clear that, with all other factors remaining same, (a) the walls of thinner channels have smaller effective slip length, and (b) shorter waves (solid) lead to lower effective slip. Moreover, the effective slip length of isolated surfaces are more sensitive to a change in wavelength of pattern than surfaces in close proximity. For either channel wall configurations, a channel separation of one wavelength appears to be large enough to be represented accurately by the theory of free shear flow over an isolated patterned surface.[30] Comparing across the panes, the effective slip of a channel wall is marginally more sensitive to patterning, if another similarly patterned wall rather than a non-slipping wall is in proximity; expectedly, this effect is discernible only for thin channels.

The remainder of the results in this section will fix the amplitude to $\alpha = 1$, which corresponds to infinitesimal zones of no-slip appearing once every period of patterning. Since, in practical situations, a hydrophobic phase with discernible slippage is inter-patterned into an hydrophilic no-slip phase, $\alpha = 1$ is of special interest. Moreover, this choice of amplitude should correspond to the largest near-wall gradients admissible by the $\beta(x)$ waveform adopted here and the current solution procedure can access this situation more conveniently and accurately than spatial discretization based numerical approaches such as Lattice-Boltzmann method, as noted by Asmolov *et al.*[30] for free shear flows.

The two panes of Fig. 5 show the variation of permeability ratio with height of channel for $\alpha = 1$ for different β_0 levels. On the left pane, corresponding to Problem I, R can be observed to approach unity if the dimensionless channel size is reduced. This means that the channel with

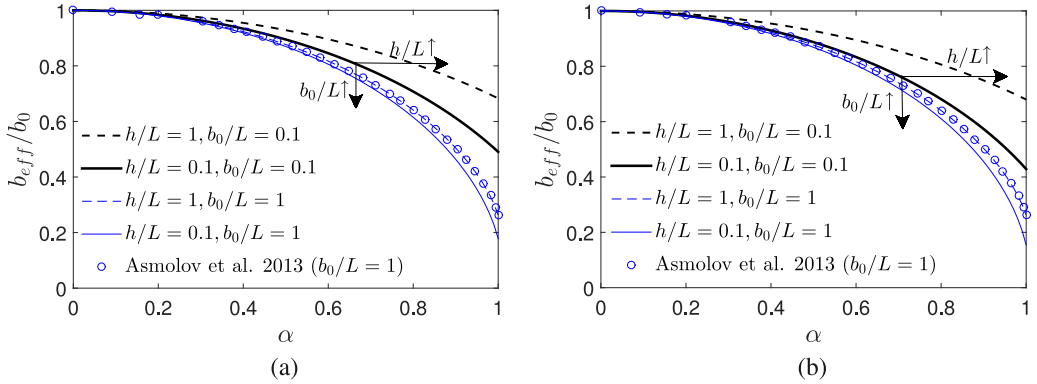


FIG. 4. Variation of the effective slip to base slip ratio of the patterned surface for $b_0/L = 1, 0.1$ and $h/L = 1, 0.1$. Symbols show free-shear flow results from Asmolov *et al.*[30] Curves plotted with the same line-thickness or colour share the same b_0/L value. Curves plotted with the same pattern (solid/dashed) share the same h/L value. Problem II is for plane channel with both walls slip-patterned (Fig. 2(b)). (a) Problem I. (b) Problem II.

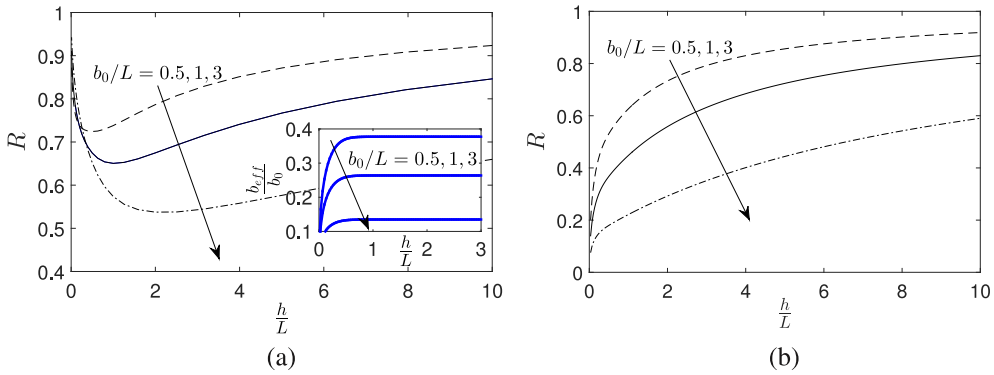


FIG. 5. Variation of the ratio of permeability of the patterned channel to that of unpatterned channel with dimensionless channel height for different values of b_0/L and $\alpha = 1$. Problem I is for a plane channel with one slip-patterned and one no slip wall (Fig. 2(a)). Problem II is for plane channel with both walls slip-patterned (Fig. 2(b)). (a) Problem I. (b) Problem II.

continuous patterns on one wall is *as permeable as a channel with unpatterned slip* in the limit of thin dimensionless channel sizes. This behaviour can be interpreted on the basis of the scaling law for thin channels $b_{eff}/h \propto \sqrt{b_0/h}$ derived in the Appendix; refer to Eq. (A9) in particular and the definition of effective permeability given by the first equality in Eq. (3). It was observed numerically, as demonstrated graphically in the supplementary material,[61] the lubrication-theory-based scaling law mentioned above is satisfied by the fully resolved semi-analytical model, despite the requirement $h/L \to 0$ of lubrication theory.

The scaling of effective slip in channels with sinusoidal patterns can be contrasted with the scaling $b_{eff}/h \propto \phi_2/\phi_1$[37,47] observed in thin channels with stick-slip patterns of area fractions ϕ_2 for the finite slip phase and ϕ_1 for the no-slip phase. It follows by using this scale in the first equality in Eq. (3), K_{eff} of a plane channel with discontinuous pattern of non-zero no-slip-phase fraction on one wall and no slip on the other wall remains bounded at a value smaller than $K_{eff} = 4$ for a channel with unpatterned slip, even in the limit of thin channel sizes. This means, a channel with discontinuous patterns on one wall *can never be as permeable as a channel with unpatterned slip* in the limit of thin dimensionless channel sizes, unlike a channel with continuous patterns. This can be construed to be an important advantage of using continuous slippage patterns in thin channels. The advantages of continuous sinusoidal patterning over stick-slip stripes in the thick channel limit, i.e., for free shear flow are discussed by Asmolov *et al.*[30]

It is important to note that the scaling law between b_{eff} and h is same for Problem II; the leading terms of Eqs. (A9) and (A11) differ only in a pre-factor. Consequently, if made thin enough, the channel in Problem II will become *infinitely permeable* compared to a no-slip channel. However, relative to a channel with uniformly slipping walls, as revealed by the corresponding value of R in Fig. 5(b), its permeability will be *infinitesimally small*. For a similar channel with a discontinuous pattern having a finite area fraction of a no-slip phase, the permeability on sufficient miniaturization can only become a finite wall-separation independent multiple of that in the corresponding no-slip channel.[37] Again, this can be construed to be an advantage of continuous sinusoidal patterns.

For the channel with one wall slip, a minimum appears at $h \sim b_0$ for every level of base slip. This suggests that, for a given patterned surface, spacing the other microchannel wall at $h \sim b_0$ as opposed to $h \gg b_0$ and $h \ll b_0$ has a penalty of accentuating the deleterious effects of patterning on permeability. Therefore, there is a certain advantage to channels with small enough thickness values (perhaps "nanochannels" from dimensional perspective), in terms of the fact that in this limit, the frictional resistance of an one-wall-patterned channel approaches that of the corresponding un-patterned but uniformly slipping channel of the same degree of slip. Note that, however, as revealed by the inset inside the left pane of Fig. 5, the dimensionless slip b_{eff}/b_0 decreases as channel height is reduced, going down ultimately to zero.

It was found that h/L location and the value of the minimum R seen in the left pane of Fig. 5 can be predicted in certain limiting situations by the two types of analyses described sequentially as follows:

A. Large base slip (b_0) to pattern wavelength (L) ratio

In such a situation, for every b_0/L value, as revealed by the inset to Fig. 5(a), the ratio of effective slip length to base slip of the patterned channel wall (b_{eff}/b_0) saturates to a value p at large enough h/L; here $p = \lim_{h/L\to\infty} b_{eff}/b_0$. As indicated earlier, the limit $h/L \to \infty$ corresponds to free shear flow. For smaller α, a similar behaviour with larger values of p was observed (not shown). In the special case of $\alpha = 1$, a closed form estimate of p is available from the free-shear flow studied by Ref. 45; in the current notation, it takes the form $p(\beta_0) = \frac{1}{2\pi\beta_0}\mathrm{E}_1[\frac{1}{2\pi\beta_0}]\mathrm{Exp}[\frac{1}{2\pi\beta_0}]$. Here $E_1(x) = \int_x^\infty \exp(-t)/t\,dt$ is the exponential integral. For specific β_0 values such as 1 and 3, either the inset in Fig. 5(a) can be used to read off p. Observation of the inset shows that the saturation level $p(\beta_0)$ has already been reached even at $h/L \simeq 1$; in other words, spacing the channel one wavelength or more apart allows the patterned walls to function nearly as isolated plates in free shear. Therefore, except in the case of small h/L values, $b_{eff} = pb_0$ can be substituted the first equality of Eq. (5) giving

$$R = \frac{(1+\lambda\beta_0)(1+4p\lambda\beta_0)}{(1+p\lambda\beta_0)(1+4\lambda\beta_0)}. \tag{39}$$

With respect to the dimensionless channel height ($\frac{1}{\lambda}$), this function is minimized at $\frac{1}{\lambda} = 2\sqrt{p}\beta_0$ to a value of

$$\min(R) = R\left(\frac{1}{\lambda} = 2\sqrt{p}\beta_0\right) = \left(\frac{1+2\sqrt{p}}{2+\sqrt{p}}\right)^2. \tag{40}$$

For example, for $b_0/L = 1$, $p = 0.2638$; the h/L location and the value of the minimum could be estimated to be equal to 1.027 and 0.6505, respectively, using Eq. (40). Comparing with the minimum in the actual numerical data, the corresponding relative errors involved in these analytical predictions are 0.7% and 0.003%, respectively. Expectedly, the minima were identified even more accurately when b_0/L values larger than unity (such as the third curve in the same pane) were investigated.

As $\beta_0 = b_0/L$ is increased, the location of the minimum $2\sqrt{p}\beta_0$ moves to the right (despite the decrease of p), i.e., to larger h/L values. The corresponding R can thereby be predicted through Eq. (40) to become lower and lower in magnitude until achieving its lowest permissible value of $R = 1/4$ when $p \to 0$. This means when $L \ll h \ll b_0$ and $\alpha = 1$, the slipping wall of the channel essentially behaves like the non-slipping wall.

B. Small base slip (b_0) to pattern wavelength (L) ratio

It can be noted that a small $\beta_0 = b_0/L$ may correspond to moderate slip to channel height value ($\lambda\beta_0 \sim O(1)$) if $\lambda \to \infty$, *for small channel height to wavelength ratios*. The lubrication theory estimate of Eq. (A10) is available to represent this limit. Minimizing the right hand side of this Eq. with respect to the single independent variable $\lambda\beta_0$, a minimum of 0.769 occurs at $\lambda\beta_0 = 2.723$. This means that lubrication theory predicts for low enough β_0/L and thereby low enough h/L, $\min(R) = \simeq 77\%$ should occur at $h = 0.367b_0$. As an example, using $b_0/L = 0.1$ in the fully resolved solution procedure revealed that this estimate is in error by ~3.3% in locating the minimizing height and by 0.19% in finding the minimum R.

The ratio R being interpreted as permeability relative to an unpatterned channel, the discussion regarding the appearance of a minimum R in Problem I can be summarized as follows. A penalty in R can be avoided either by choosing small or large channel heights ($h \ll b_0$ or $h \gg \beta_0$) for a pattern of given wavelength. The lowest R is recorded with short wavelengths and large channel spacings. For sufficiently long wave patterns, the minimum in R appears at $h \simeq 0.367b_0$ and involves a milder

penalty of ~23% degradation from the value of unpatterned channel permeability. A penalty in R can be avoided either by choosing small or large channel heights ($h \ll b_0$ or $h \gg \beta_0$).

It was observed from the numerical results that for moderately short wavelengths (corresponding to moderately small b_0/L values), none of the above two closed form estimates $b_0/h = 1/(2\sqrt{p}), 2.723$, corresponding to small and large wavelengths represents the location of the minimum (and its value) with adequate accuracy. The curve corresponding to $b_0/L = 0.5$ in the left pane of Fig. 5 represents such a situation. This situation emphasizes the necessity of the full solution procedure for arbitrary channel separations as described here.

Returning now to Fig. 5(b), the patterned to unpatterned channel permeability ratio increases monotonically with channel height for channels with two patterned walls. While this means, there is no advantage to be derived in Problem II in terms of R by making the channel thinner, it should also be noted that because of the scaling law in Eq. (A11), $K_{eff} = 1 + 6b_{eff}/h$ still becomes large in the thin channel limit. It may also be recalled from the literature that for a thin channel, the scaling of effective slip in case of a channel with discontinuous patterns on both walls remains the same, *viz.,* $b_{eff} \propto h\phi_2/\phi_1$ in Problem II, see, for example, Eq. (5b) of Feuillebois *et al.*[37] Note that these results also follow from Eq. (A7), as discussed in the Appendix. Therefore, K_{eff} of such channels remains finite in the thin channel limit. Thus, thin channels with continuous patterns have superior permeability not only compared to their thicker counterparts, but also compared to channels of same size with discontinuous patterns.

It is interesting to note that this advantageous behaviour ($b_{eff}/h \to \infty$ as $h/L \to 0$) of thin channels with continuous slip pattern over thin channels with a discontinuous square slip-wave pattern (where $b_{eff}/h \sim O(1)$ as $h/L \to 0$) carries over even to channels where a 180° phase-mismatch exists between the top and bottom wall slip waves. As can be inferred from closed-form expressions given in the Appendix, a 180° phase-mismatch enhances the permeability of channel, regardless of whether the patterns are continuous or stick-slip. On the basis of Eq. (A7), it was found that for a thin enough channel, an arbitrary phase-mismatch of θ results in an increase the permeability (and the effective slip length) of the channel; the increase is monotonic in $0 < \theta \leq \pi$. It was further found that the sensitivity of b_{eff}/h to a differential angular misalignment is smallest near $\theta = 0, \pi$ and highest near $\theta = \pi/2$. Representative graphical data on b_{eff}/h vs. θ dependence, from which these observations may be discerned, are shown in the supplementary material. A figure is also provided in the supplementary material[61] that shows that both for completely phase-matched and completely phase-mismatched cosine slip waves, as the average slip b_0/h varies, the effective slip b_{eff}/h exceeds the effective slip of square waves of corresponding phase and the same average slip. The square waves show a saturation in b_{eff}/h for large b_0/h, which the cosine wave does not.

Concluding the discussion on the global measures of slip, it can be emphasized that in either problems, the effective slip length b_{eff} and the dimensionless permeability (K_{eff}) were found to increase if surfaces with higher degree of average slip (b_0) were used, unlike the normalized measures b_{eff}/b_0 and R. The dependence of the normalized measures on b_0 is reflecting the fact that the

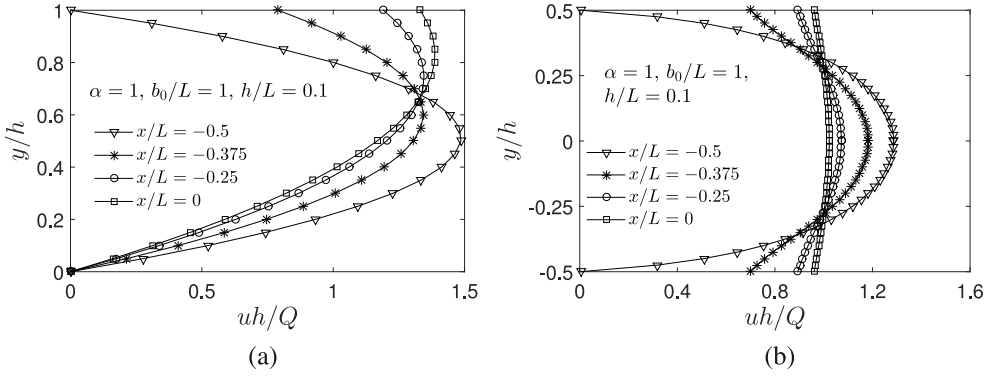


FIG. 6. The cross-channel (y) variation of the stream-wise velocity (u) at different axial locations on the channel top wall. Input parameters are $\alpha = 1$, $b_0/L = 1$, and $h/L = 0.1$. Problem I is for a plane channel with one slip-patterned and one no slip wall (Fig. 2(a)). Problem II is for plane channel with both walls slip-patterned (Fig. 2(b)). (a) Problem I. (b) Problem II.

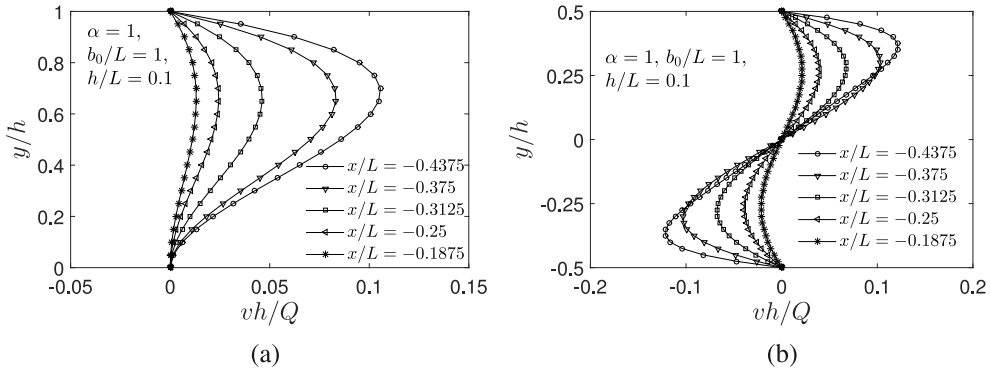


FIG. 7. The cross-channel (y) variation of the cross-channel velocity (v) at different axial locations. Input parameters are $\alpha = 1$, $b_0/L = 1$, and $h/L = 0.1$. Problem I is for a plane channel with one slip-patterned and one no slip wall (Fig. 2(a)). Problem II is for plane channel with both walls slip-patterned (Fig. 2(b)). (a) Problem I. (b) Problem II.

slip waveform given by Eq. (1) is such that increasing b_0 also increases the overall slip variation ($2\alpha b_0$). This is also consistent with the leading order long wave behaviour $b_{eff} \propto \sqrt{b_0}$ applicable to thin channels obtained from Eqs. (A9) and (A11). In the remainder of this section, features of the local velocity field will be described.

Fig. 6 shows the variation of u (x-component of velocity) along the height of the channel at different points in x-direction for transverse flow in a channel for $b_0/L = 1$ and $h/L = 0.1$. Fig. 7 shows the variation of v (y-component of velocity) along the height of the channel at different points in X-direction for transverse flow in a channel. Fig. 8 shows the streamlines of flow. As seen in Fig. 6, two-thirds way into the channel in y direction from the wall for the Problem I and about one-fifth and four-fifths way from the wall in Problem II, there exists region(s) where the axial variation in u is very small. It was also observed (not shown) that as h/L value was increased with other parameters set as in Fig. 7, the secondary velocity (the v component) engendered by the pattern at any cross-sectional plane tended to localize near the channel wall. Thus, the wavelength, if it is small enough, controls even the cross-channel variations, as expected based on scaling considerations.[35] Increasing the average slip length (larger b_0/L values), with all other parameters fixed as in Figs. 6 and 7, leads to the strong axial variations in u to localize preferentially near the no-slip spots, with very weak variations in the high-slip zones.

Fig. 8 show the streamlines of the flow in Problems I and II over a periodic span of length $2L$, as obtained from equi-spaced level surfaces of the stream-function given by Eq. (18). The no-slip spots on the $\alpha = 1$ pattern cause the streamlines to bend away from the wall significantly, thereby "focusing" the flow. In general, in regions where slip increases/decreases in the stream-wise

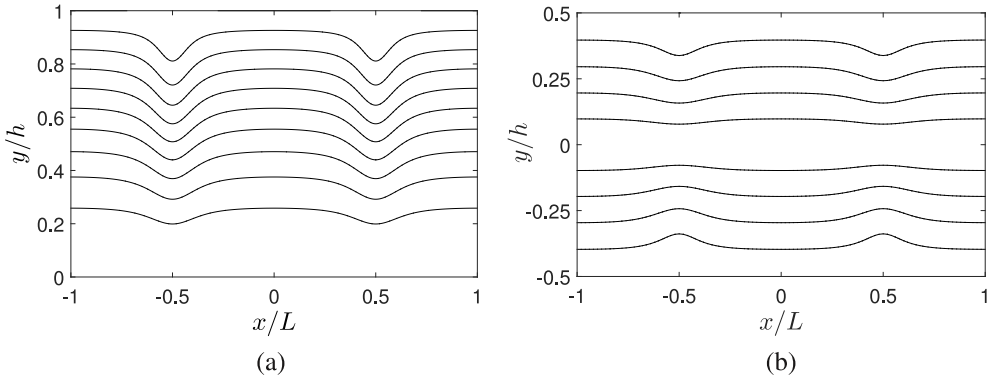


FIG. 8. The streamlines of flow. Input parameters are $\alpha = 1$, $b_0/L = 1$, and $h/L = 0.1$. Problem I is for a plane channel with one slip-patterned and one no slip wall (Fig. 2(a)). Problem II is for plane channel with both walls slip-patterned (Fig. 2(b)). (a) Problem I. (b) Problem II.

direction, the streamlines bend toward/away from the wall. On the left pane, there is relatively low flow close to either walls. Expectedly, unlike the zone near the bottom no-slip wall, the flow near the slipping wall becomes significantly stronger on lowering the pattern amplitude.

IV. CONCLUSIONS

The pressure-driven flow through a plane channel of arbitrary wall separation having continuous pattern(s) of sinusoidally varying slip length of arbitrary wavelength and amplitude on one/both walls has been studied through a spectrally accurate semi-analytical mathematical model. In addition, a lubrication theory has been developed for the sinusoidal slip waveform, not only to test against closed-form results the long-wave limit of the semi-analytical theory, but also to understand the scaling behaviours typical of continuous slip waveforms. For a channel with a given pattern-averaged slip length, increasing the wave-number and amplitude of the pattern adversely affects the relative improvement in hydraulic permeability expected of a slipping channel over a channel with no-slip walls. The effective slip length of the wall becomes a smaller fraction of the average slip length, as the latter is increased.

As a consequence of a weaker scaling of the effective slip length with channel size unique to sinusoidal rather than discontinuous stick-slip patterns,[32,37,47] on sufficient miniaturization, the permeability of a channel with sinusoidal variations will always surpass that of a channel whose walls have discontinuous patterns of finite solid area fraction. In contrast with discontinuous patterns, (a) in the case where the channel has one no-slip wall and one sinusoidally patterned wall, the channel permeability in the thin channel limit approaches the permeability of an unpatterned channel with uniform slippage equalling the pattern-averaged slip length. (b) In the case where both walls of the channel are patterned, a channel with continuous patterns can be infinitely more permeable than a channel whose all walls are non-slipping.

A new measure of channel performance termed permeability ratio has been developed in this work. The permeability ratio is the multiplicative factor by which the permeability of a channel with patterned wall(s) differs from that of a hypothetical reference channel having a uniform slip length equalling the period-averaged slip length on the corresponding wall(s). In case of a channel with one slip-patterned and one non-slipping wall, a minimum appears in the channel size dependence of the permeability ratio at an intermediate channel size. Analytical expressions for tracking the location and size of this minimum when the wavelength of the pattern is changed have been provided, which are shown to be accurate for $b_0/L \sim 1$ or higher on one hand, and $b_0/L \ll 1$ on the other hand. For example, with thin enough channels (numerically for about $h/L < 0.1$) and long enough pattern wavelengths (numerically about $L \geq b$), a worst case penalty of about 23% due to patterning arises when the average slip of the channel is about 2.7 times the channel size. This prediction is a closed form result from the lubrication theory.

Previous work in the literature that has dealt with confined pressure-driven flows with slip-patterned walls has mostly either studied the limit of thin channels[34,37] or thick channels[30,43,46] and/or utilized discontinuous slip/no-slip waveforms.[32,37,47] In studying the effect of the sinusoidal slip waveform, special attention in this study has been given to the case of largest permissible amplitude of the pattern, whence infinitesimal zones of no slip appear on the surface. This limit which results in the maximum deleterious effects of patterning due to largest gradients has earlier posed challenge to several works in the literature using a similar slip waveform in confined flows.[33,42,66,67] Two other works[30,45] access this amplitude limit for sinusoidal waveforms, but apply only to the unconfined free-shear flow (thick channel limit). The current work bridges the gap between thin and thick channel limits, by considering arbitrary separation between the walls. In the special situations of thin and thick channels, respectively, the predictions of the model are found to be consistent with lubrication theory, as developed in the Appendix and the above-referred studies pertaining to free shear flow. Detailed analysis and comparison of channel configurations with similar and dissimilar walls (Problems I and II) are also an important contribution of the current study. Lubrication theory has also been used to study the effect of misalignment between slip patterns,[34,68] as represented by a phase angle between the wall pattern; certain analytical results from Ref. 34 emerge as special cases of these analysis.

The current work can be generalized to arbitrary periodic waveforms. Flow anisotropy effects of patterned slip in nanochannels can also be studied, taking advantage of results for flow along the patterns.[59] The pattern-averaged slip length (b_0) is an input parameter to the theoretical model and the measure termed permeability ratio developed in this work. Although average slip is simpler to define than effective slip, it is currently more difficult to measure than effective slip length itself.[6] With progress in microscopy and flow visualization,[8,52] it may be possible to calculate this input parameter by directly averaging the measured local slip. Study of the shape and deformation of interfaces[69–72] along with topographical details and modelling gas phase viscous dissipation may be necessary to build better correspondence with realistic experimental situations.[8]

ACKNOWLEDGMENTS

Financial assistance from the SERB division, Department of Science and Technology, India (Sanction Letter No. SB/FTP/ETA-142/2012) is acknowledged by SD.

APPENDIX: LUBRICATION THEORY ESTIMATES OF THE EFFECTIVE PERMEABILITY FACTOR

Consider a channel with slip length distributions $b_1(x)$ and $b_2(x)$ on bottom and top walls, respectively. Following the scaling approach of classical lubrication theory,[73] the equations of steady incompressible Stokes flow, the constraint of prescribed flow-rate, and the slip boundary conditions on either walls are first expressed in the dimensionless variables $\xi = x/L$, $\eta = y/h$, $u = (Q/h)\overline{U}$, $v = (Q/L)\overline{V}$, $p = (QL/h^3)\overline{P}$,

$$\left(\frac{1}{\lambda}\right)^2 \frac{\partial^2 \overline{U}}{\partial \xi^2} + \frac{\partial^2 \overline{V}}{\partial \eta^2} = \frac{\partial \overline{P}}{\partial \xi}, \tag{A1}$$

$$\left(\frac{1}{\lambda}\right)^4 \frac{\partial^2 \overline{V}}{\partial \xi^2} + \left(\frac{1}{\lambda}\right)^2 \frac{\partial^2 \overline{V}}{\partial \eta^2} = \frac{\partial \overline{P}}{\partial \eta}, \tag{A2}$$

$$\int_0^1 \overline{U}\, d\eta = 1, \tag{A3}$$

$$-\lambda\beta_1 \frac{\partial \overline{U}}{\partial \eta} + \overline{U} = 0, \tag{A4}$$

$$\lambda\beta_2 \frac{\partial \overline{U}}{\partial \eta} + \overline{U} = 0. \tag{A5}$$

Lubrication theory is used to study the limit of these equations as $\lambda \to \infty$, when values are prescribed for the effective slip to channel height ratios $\lambda\beta_1$ and $\lambda\beta_2$. In this limit, solving the resultant equations for $\overline{U}$ and the pressure gradient gives

$$\frac{d\overline{P}}{d\xi} = -12 \frac{\lambda\beta_1 + \lambda\beta_2 + 1}{4\lambda\beta_1(3\lambda\beta_2 + 1) + (4\lambda\beta_1 + 1)}. \tag{A6}$$

The overall pressure drop $\Delta\overline{P} = \overline{P}(0,\eta) - \overline{P}(1,\eta)$ is calculated on integrating this equation in ξ,

$$\Delta\overline{P} = 12 \int_0^1 \frac{\lambda\beta_1 + \lambda\beta_2 + 1}{4\lambda\beta_1(3\lambda\beta_2 + 1) + (4\lambda\beta_1 + 1)}\, d\xi. \tag{A7}$$

For a channel with one no-slip wall and one wall slipping with the sinusoidal distribution of slip used in the current work, $\beta_1 = 0$ and $\beta_2 = \beta_0(1 + \alpha\cos(2\pi\xi))$. For a channel with both walls slipping with the sinusoidal distribution of slip used in the current work, $\beta_2 = \beta_1 = \beta_0(1 + \alpha\cos(2\pi\xi))$. Since for a given flow-rate, $R = \frac{\Delta\overline{P}_{\alpha=0}}{\Delta\overline{P}_{\alpha\neq 0}}$, Eq. (A7) can be used to get following closed form estimates.

In case of Problem I,

$$R^{LT} = K_{eff}^{LT}\left(\frac{1+\lambda\beta_0}{1+4\lambda\beta_0}\right) = \left[\frac{4\sqrt{(1+4(1+\alpha)\lambda\beta_0)\,(1+4(1-\alpha)\lambda\beta_0)}}{3+\sqrt{(1+4(1+\alpha)\lambda\beta_0)\,(1+4(1-\alpha)\lambda\beta_0)}}\right]\left(\frac{1+\lambda\beta_0}{1+4\lambda\beta_0}\right). \quad \text{(A8)}$$

The superscript LT on the dimensionless permeability (K_{eff}) and the permeability ratio (R) emphasizes the long-wave approximation involved in lubrication theory (LT). The effective slip length in channel size units ($\lambda\beta_{eff}$) of the wall with slippage in Fig. 2(a) can be calculated in closed form using Eq. (3).[37] For future reference, we note that in the important situation of $\alpha = 1$ and large enough $\lambda b_0 = \frac{b_0}{h}$, the corresponding expressions for $b_{eff}/h = \lambda\beta_{eff}$ can be given in the following asymptotic form:

$$\frac{b_{eff}}{h} = \sqrt{\frac{b_0}{2h}} - \frac{1}{4} + O[\frac{h}{b_0}]^{1/2}. \quad \text{(A9)}$$

In case of Problem II, Eq. (A7) gives

$$R^{LT} = \frac{K_{eff}^{LT}}{1+6\lambda\beta_0} = \frac{\sqrt{(1+6(1+\alpha)\lambda\beta_0)\,(1+6(1-\alpha)\lambda\beta_0)}}{1+6\lambda\beta_0}. \quad \text{(A10)}$$

The effective slip length in channel size units ($\lambda\beta_{eff}$) of either of the slipping walls in Fig. 2(b) can be calculated using Eq. (3) $\lambda\beta_{eff} = \frac{K_{eff}-1}{6}$. It can be noted that Eq. (28) of Ng and Zhou[34] can be recovered on setting $\alpha = 1$ in Equation (A10).

For future reference, we note that in the important situation of $\alpha = 1$ and large enough $\lambda b_0 = \frac{b_0}{h}$, the corresponding expressions for $b_{eff}/h = \lambda\beta_{eff}$ can be given the following asymptotic form:

$$\frac{b_{eff}}{h} = \sqrt{\frac{b_0}{3h}} - \frac{1}{6} + O[\frac{h}{b_0}]^{1/2}. \quad \text{(A11)}$$

The first terms in Eqs. (A9) and (A11) justify the scaling law $b_{eff} \propto \sqrt{hb_0}$ for thin channels and long wave patterns, mentioned in the main text.

Eq. (A7) can be used for other functional forms of $\beta_1(X)$ and $\beta_2(X)$, including the important case of certain discontinuous functions. For example, if one or more of the channel walls have alternating slip no slip stripes, the pressure drop in the resultant Stokes flow is represented quite accurately by specifying β_1 or β_2 piecewise in Eq. (A7), except for infinitesimal zones form small enough h/L near the discontinuities.[73] As an example, for stripes with slip length β of area fraction ϕ_2 alternative no-slip stripes of area fraction $\phi_1 = 1 - \phi_2$, the results of Feuillebois *et al.*,[37] Schmieschek *et al.*,[47] namely, $\frac{b_{eff}}{h} = \frac{\phi_2 b_0/h}{1+4\phi_1 b_0/h}$ for one wall non-slipping and $\frac{b_{eff}}{h} = \frac{\phi_2 b_0/h}{1+6\phi_1 b_0/h}$ are recovered from Eq. (A7).

Phase-shifted waveforms can also be studied using Eq. (A7). For example, $\beta_1 = \beta_0(1 + \alpha\cos(2\pi\xi))$ and $\beta_2 = \beta_0(1 + \alpha\cos(2\pi\xi + \theta))$ can be used in Eq. (A7) to study the effect of a misalignment between top and bottom wall patterns resulting in a phase-shift θ. When $\theta = \pi$, a closed form expression $K^{LT} = (6\lambda\beta_0 + 1)\sqrt{1 - \frac{12\alpha^2\lambda^2\beta_0^2}{(8\lambda\beta_0+1)(6\lambda\beta_0+1)}}$ is obtained for the dimensionless permeability, with $b_{eff/h} = \frac{K^{LT}-1}{6}$. It can be noted that Eq. (29) of Ng and Zhou[34] can be recovered on setting $\alpha = 1$ in this expression. It is interesting to compare the effective slip length of a square stick-slip wave (50% area fraction with slip length b_0) with π phase shift with its continuous counterpart. For the latter, Eq. (A7) gives $\frac{b_{eff}}{h} = \frac{b_0/h}{2(1+b_0/h)}$. Note that from the closed-form expressions above, it can be inferred that, even for a phase-mismatch of π, for large values of b_0/h, b_{eff}/h becomes unbounded for continuous patterns and remains finite for discontinuous patterns.

[1] G. Karniadakis, A. Beskok, and N. Aluru, *Microflows and Nanoflows* (Springer, New York, 2006).
[2] M. M. Denn, "Extrusion instabilities and wall slip," Annu. Rev. Fluid Mech. **33**(1), 265–287 (2001).
[3] D. C. Tretheway and C. D. Meinhart, "Apparent fluid slip at hydrophobic microchannel walls," Phys. Fluids **14**(3), L9–L12 (2002).
[4] C. Cottin-Bizonne, S. Jurine, J. Baudry, J. Crassous, F. Restagno, and E. Charlaix, "Nanorheology: An investigation of the boundary condition at hydrophobic and hydrophilic interfaces," Eur. Phys. J. E **9**(1), 47–53 (2002).

[5] N. V. Priezjev and S. M. Troian, "Molecular origin and dynamic behavior of slip in sheared polymer films," Phys. Rev. Lett. **92**(1), 018302 (2004).
[6] E. Lauga, M. Brenner, and H. A. Stone, "Microfludics: The no-slip boundary condition," in *Handbook of Experimental Fluid Mechanics*, edited by C. Tropea, A. Yarin, and J. F. Fouss (Springer, New York, 2007), Chap. 19, pp. 1219–1240.
[7] P. Wu and R. Qiao, "Physical origins of apparently enhanced viscosity of interfacial fluids in electrokinetic transport," Phys. Fluids **23**(7), 072005 (2011).
[8] O. I. Vinogradova, K. Koynov, A. Best, and F. Feuillebois, "Direct measurements of hydrophobic slippage using double-focus fluorescence cross-correlation," Phys. Rev. Lett. **102**(11), 118302 (2009).
[9] A. Maali, Y. Pan, B. Bhushan, and E. Charlaix, "Hydrodynamic drag-force measurement and slip length on microstructured surfaces," Phys. Rev. E **85**, 066310 (2012).
[10] M. K. Chaudhury and G. M. Whitesides, "How to make water run uphill," Science **256**(5063), 1539–1541 (1992).
[11] D. Quéré, "Wetting and roughness," Annu. Rev. Mater. Res. **38**, 71–99 (2008).
[12] C. Lee, C.-H. Choi, and C.-J. C. Kim, "Structured surfaces for a giant liquid slip," Phys. Rev. Lett. **101**, 064501 (2008).
[13] J. Ou, B. Perot, and J. P. Rothstein, "Laminar drag reduction in microchannels using ultrahydrophobic surfaces," Phys. Fluids **16**(12), 4635–4643 (2004).
[14] H. Stone, A. Stroock, and A. Ajdari, "Engineering flows in small devices," Annu. Rev. Fluid Mech. **36**, 381–411 (2004).
[15] C.-H. Choi, U. Ulmanella, J. Kim, C.-M. Ho, and C.-J. Kim, "Effective slip and friction reduction in nanograted superhydrophobic microchannels," Phys. Fluids **18**(8), 087105 (2006).
[16] E. Karatay, A. S. Haase, C. W. Visser, C. Sun, D. Lohse, P. A. Tsai, and R. G. Lammertink, "Control of slippage with tunable bubble mattresses," Proc. Natl. Acad. Sci. U. S. A. **110**(21), 8422–8426 (2013).
[17] Y. Ren and D. Stein, "Slip-enhanced electrokinetic energy conversion in nanofluidic channels," Nanotechnology **19**(19), 195707 (2008).
[18] M. Napoli, J. C. T. Eijkel, and S. Pennathur, "Nanofluidic technology for biomolecule applications: A critical review," Lab Chip **10**(8), 957–985 (2010).
[19] S. Datta and J. Choudhary, "Effect of hydrodynamic slippage on electro-osmotic flow in zeta potential patterned nanochannels," Fluid Dyn. Res. **45**(5), 055502 (2013).
[20] M. Z. Bazant and O. I. Vinogradova, "Tensorial hydrodynamic slip," J. Fluid Mech. **613**, 125–134 (2008).
[21] P. Gao and J. J. Feng, "Enhanced slip on a patterned substrate due to depinning of contact line," Phys. Fluids **21**(10), 102102 (2009).
[22] A.-L. Vayssade, C. Lee, E. Terriac, F. Monti, M. Cloitre, and P. Tabeling, "Dynamical role of slip heterogeneities in confined flows," Phys. Rev. E **89**, 052309 (2014).
[23] O. I. Vinogradova and A. V. Belyaev, "Wetting, roughness and flow boundary conditions," J. Phys.: Condens. Matter **23**(18), 184104 (2011).
[24] T. V. Nizkaya, E. S. Asmolov, and O. I. Vinogradova, "Gas cushion model and hydrodynamic boundary conditions for superhydrophobic textures," Phys. Rev. E **90**(4), 043017 (2014).
[25] A. Steinberger, C. Cottin-Bizonne, P. Kleimann, and E. Charlaix, "High friction on a bubble mattress," Nat. Mater. **6**, 665–668 (2007).
[26] A. D. Stroock, S. K. Dertinger, G. M. Whitesides, and A. Ajdari, "Patterning flows using grooved surfaces," Anal. Chem. **74**(20), 5306–5312 (2002).
[27] E. S. Asmolov, A. L. Dubov, T. V. Nizkaya, A. J. C. Kuehne, and O. I. Vinogradova, "Principles of transverse flow fractionation of microparticles in superhydrophobic channels," Lab Chip **15**, 2835–2841 (2015).
[28] J. Philip, "Flows satisfying mixed no-slip and no-shear conditions," Z. Angew. Math. Phys. **23**(3), 353–372 (1972).
[29] S. S. Bahga, O. I. Vinogradova, and M. Z. Bazant, "Anisotropic electro-osmotic flow over super-hydrophobic surfaces," J. Fluid Mech. **644**, 245–255 (2010).
[30] E. S. Asmolov, S. Schmieschek, J. Harting, and O. I. Vinogradova, "Flow past superhydrophobic surfaces with cosine variation in local slip length," Phys. Rev. E **87**(2), 023005 (2013).
[31] S. C. Hendy, M. Jasperse, and J. Burnell, "Effect of patterned slip on micro- and nanofluidic flows," Phys. Rev. E **72**, 016303 (2005).
[32] F. Feuillebois, M. Z. Bazant, and O. I. Vinogradova, "Transverse flow in thin superhydrophobic channels," Phys. Rev. E **82**, 055301 (2010).
[33] U. Ghosh and S. Chakraborty, "Patterned-wettability-induced alteration of electro-osmosis over charge-modulated surfaces in narrow confinements," Phys. Rev. E **85**, 046304 (2012).
[34] C.-O. Ng and Q. Zhou, "Electro-osmotic flow through a thin channel with gradually varying wall potential and hydrodynamic slippage," Fluid Dyn. Res. **44**(5), 055507 (2012).
[35] C. Ybert, C. Barentin, C. Cottin-Bizonne, P. Joseph, and L. Bocquet, "Achieving large slip with superhydrophobic surfaces: Scaling laws for generic geometries," Phys. Fluids **19**(12), 123601 (2007).
[36] A. Ajdari, "Transverse electrokinetic and microfluidic effects in micropatterned channels: Lubrication analysis for slab geometries," Phys. Rev. E **65**(1), 016301 (2001).
[37] F. Feuillebois, M. Z. Bazant, and O. I. Vinogradova, "Effective slip over superhydrophobic surfaces in thin channels," Phys. Rev. Lett. **102**, 026001 (2009).
[38] E. Lauga and H. A. Stone, "Effective slip in pressure-driven stokes flow," J. Fluid Mech. **489**, 55–77 (2003).
[39] C. Wang, "Flow over a surface with parallel grooves," Phys. Fluids **15**(5), 1114–1121 (2003).
[40] K. Kamrin, M. Z. Bazant, and H. A. Stone, "Effective slip boundary conditions for arbitrary periodic surfaces: The surface mobility tensor," J. Fluid Mech. **658**, 409–437 (2010).
[41] L. M. Hocking, "A moving fluid interface on a rough surface," J. Fluid Mech. **76**, 801–817 (1976).
[42] J. Choudhary, S. Datta, and S. Jain, "Effective slip in nanoscale flows through thin channels with sinusoidal patterns of wall wettability," Microfluid. Nanofluid. **18**, 931–942 (2014).
[43] A. V. Belyaev and O. I. Vinogradova, "Effective slip in pressure-driven flow past super-hydrophobic stripes," J. Fluid Mech. **652**, 489–499 (2010).

[44] E. S. Asmolov and O. I. Vinogradova, "Effective slip boundary conditions for arbitrary one-dimensional surfaces," J. Fluid Mech. **706**, 108–117 (2012).
[45] P. Six and K. Kamrin, "Some exact properties of the effective slip over surfaces with hydrophobic patternings," Phys. Fluids **25**(2), 021703 (2013).
[46] E. S. Asmolov, J. Zhou, F. Schmid, and O. I. Vinogradova, "Effective slip-length tensor for a flow over weakly slipping stripes," Phys. Rev. E **88**(2), 023004 (2013).
[47] S. Schmieschek, A. V. Belyaev, J. Harting, and O. I. Vinogradova, "Tensorial slip of superhydrophobic channels," Phys. Rev. E **85**, 016324 (2012).
[48] C.-O. Ng and H. C. W. Chu, "Electrokinetic flows through a parallel-plate channel with slipping stripes on walls," Phys. Fluids **23**(10), 102002 (2011).
[49] L. G. Leal, *Advanced Transport Phenomena: Fluid Mechanics and Convective Transport Processes* (Cambridge University Press, 2007).
[50] T. V. Nizkaya, E. S. Asmolov, and O. I. Vinogradova, "Flow in channels with superhydrophobic trapezoidal textures," Soft Matter **9**(48), 11671–11679 (2013).
[51] D. Dilip, N. K. Jha, R. N. Govardhan, and M. Bobji, "Controlling air solubility to maintain cassie state for sustained drag reduction," Colloids Surf., A **459**, 217–224 (2014).
[52] Z. Li, L. Deramo, C. Lee, F. Monti, M. Yonger, P. Tabeling, B. Chollet, B. Bresson, and Y. Tran, "Near-wall nanovelocimetry based on total internal reflection fluorescence with continuous tracking," J. Fluid Mech. **766**, 147–171 (2015).
[53] U. Ghosh and S. Chakraborty, "Electrokinetics over charge-modulated surfaces in the presence of patterned wettability: Role of the anisotropic streaming potential," Phys. Rev. E **88**(3), 033001 (2013).
[54] C. Zhao and C. Yang, "Electro-osmotic flows in a microchannel with patterned hydrodynamic slip walls," Electrophoresis **33**(6), 899–905 (2012).
[55] C. Cottin-Bizonne, J.-L. Barrat, L. Bocquet, and E. Charlaix, "Low-friction flows of liquid at nanopatterned interfaces," Nat. Mater. **2**(4), 237–240 (2003).
[56] J. Davies, D. Maynes, B. Webb, and B. Woolford, "Laminar flow in a microchannel with superhydrophobic walls exhibiting transverse ribs," Phys. Fluids **18**(8), 087110 (2006).
[57] C.-O. Ng and C. Wang, "Apparent slip arising from stokes shear flow over a bidimensional patterned surface," Microfluid. Nanofluid. **8**(3), 361–371 (2010).
[58] J. Harting, C. Kunert, and J. Hyväluoma, "Lattice Boltzmann simulations in microfluidics: Probing the no-slip boundary condition in hydrophobic, rough, and surface nanobubble laden microchannels," Microfluid. Nanofluid. **8**(1), 1–10 (2010).
[59] A. Kumar, S. Datta, and D. Kalyanasundaram, "Liquid slippage in confined flows: Effect of periodic micropatterns of arbitrary pitch and amplitude," in *ASME 2016 Fifth International Conference on Micro/Nanoscale Heat Transfer* (American Society of Mechanical Engineers, 2016).
[60] P. M. Adler and H. Brenner, "Multiphase flow in porous media," Annu. Rev. Fluid Mech. **20**(1), 35–59 (1988).
[61] See supplementary material at http://dx.doi.org/10.1063/1.4959184 for derivation of Eqs. (3) and (5) through averaging of the local fluid dynamic equations.
[62] C. Canuto, M. Hussaini, A. Quarteroni, and T. Zang, *Spectral Methods in Fluid Dynamics*, Scientific Computation (Springer-Verlag, New York, Heidelberg, Berlin, 1987).
[63] J. H. Ferziger and M. Peric, *Computational Methods for Fluid Dynamics* (Springer Science & Business Media, 2012).
[64] C. M. Bender and S. A. Orszag, *Advanced Mathematical Methods for Scientists and Engineers I* (Springer Science & Business Media, 1999).
[65] R. Govindarajan and K. C. Sahu, "Instabilities in viscosity-stratified flow," Annu. Rev. Fluid Mech. **46**, 331–353 (2014).
[66] S. C. Hendy and N. J. Lund, "Effective slip boundary conditions for flows over nanoscale chemical heterogeneities," Phys. Rev. E **76**, 066313 (2007).
[67] N. J. Lund and S. C. Hendy, "Effective slip length of nanoscale mixed-slip surfaces," ANZIAM J. **50**(03), 381–394 (2009).
[68] T. V. Nizkaya, E. S. Asmolov, J. Zhou, F. Schmid, and O. I. Vinogradova, "Flows and mixing in channels with misaligned superhydrophobic walls," Phys. Rev. E **91**(3), 033020 (2015).
[69] D. Einzel, P. Panzer, and M. Liu, "Boundary condition for fluid flow: Curved or rough surfaces," Phys. Rev. Lett. **64**, 2269–2272 (1990).
[70] M. Sbragaglia and A. Prosperetti, "A note on the effective slip properties for microchannel flows with ultrahydrophobic surfaces," Phys. Fluids **19**(4), 043603 (2007).
[71] S. Chakraborty, T. Das, and S. Chattoraj, "A generalized model for probing frictional characteristics of pressure-driven liquid microflows," J. Appl. Phys. **102**(10), 104907 (2007).
[72] A. M. Davis and E. Lauga, "Geometric transition in friction for flow over a bubble mattress," Phys. Fluids **21**(1), 011701 (2009).
[73] M. Van Dyke, "Slow variations in continuum mechanics," Adv. Appl. Mech. **25**, 1–45 (1987).